Available online at www.sciencedirect.com
SCIENCE DIRECT®
Journal of Molecular Catalysis A: Chemical 232 (2005) 151–159
JOURNAL OF MOLECULAR CATALYSIS A: CHEMICAL
www.elsevier.com/locate/molcata

Olefin hydrogenation using diimine pyridine complexes of Co and Rh

Quinten Knijnenburg [a], Andrew D. Horton [b], Harry van der Heijden [b], T. Martijn Kooistra [a], Dennis G.H. Hetterscheid [a], Jan M.M. Smits [a], Bas de Bruin [a], Peter H.M. Budzelaar [a,*], Anton W. Gal [a]

[a] *Metal-Organic Chemistry, University of Nijmegen, Toernooiveld 1, 6525 ED Nijmegen, The Netherlands*
[b] *CTCCT/1 Chemistry and Homogeneous Catalysis Shell International Chemicals B.V., P.O. Box 38000, 1030 BN Amsterdam, The Netherlands*

Received 17 November 2004; received in revised form 16 December 2004; accepted 20 December 2004

Abstract

Square-planar cobalt diimine pyridine complexes LCoR (L = 2,6-[RN=CMe]$_2$C$_5$H$_3$N; R = *n*-C$_6$H$_{13}$ for L^{hex}, 2,6-(*i*-Pr)$_2$C$_6$H$_3$ for L^{dip}) are active in the hydrogenation of monosubstituted and disubstituted olefins; sterically more hindered trisubstituted olefins do not react. For the L^{dip}Co system, a diamagnetic hydride intermediate was observed, although a small amount of paramagnetic product is also formed upon reaction of L^{dip}CoR with H_2. DFT studies suggest a traditional hydrogenation cycle starting with LCoH, except that intermediate LCo(R)(H_2) transfers a hydrogen atom directly from H_2 to the alkyl group in a σ-bond metathesis step, without going through a discrete Co^{III} intermediate. Autoclave experiments show that conversion is not linear in catalyst intake. Diffusion limitation was ruled out as an explanation, and we propose a concentration-dependent catalyst decay. At low catalyst intake conversion rates up to 2×10^4 (mol octene/mol Co/bar/h) can be reached. Reducing the steric bulk at the imine positions (L^{dip} → L^{hex}), or changing the metal from cobalt to rhodium, do not alter the activity or specificity of the hydrogenation much. For the L^{hex}Co and L^{dip}Rh systems, no diamagnetic products corresponding to L^{dip}CoH were observed.

Keywords: Hydrogenation; DFT calculations; EPR measurements; Cobalt; Diimine pyridine

1. Introduction

Organometallic complexes of rhodium and (to a lesser extent) iridium play a prominent role in homogenous catalysis [1,2]. They owe this role mainly to their ability to switch between oxidation states +1 and +3, thus enabling a wide range of reactions, in particular hydroformylation [3,4] and hydrogenation [5,6]. The lighter group 9 congener cobalt has a preference for the +2 and +3 oxidation states, which in general prevents it from catalysing the same types of reactions. However, cobalt carbonyls are active in hydroformylation, suggesting that in combination with strong π-acceptor ligands cobalt behaves more like rhodium. The low cost and relatively low environmental impact would make cobalt a very attractive alternative for rhodium and iridium, if it could be made to perform analogously in other catalytic reactions (e.g. hydrogenation). One possible approach would be the use of a strong π-acceptor ligand that could stabilize low-spin Co^{I} while still allowing access to the Co^{III} oxidation state.

In earlier studies we have observed that the diimine pyridine ligand has the ability to accept an electron from various metal centers, forming an anion radical [7–10]. In recent work on polymerisation with cobalt diimine pyridine complexes, the groups of Gibson et al. [11] and ourselves [12] independently discovered that en route to the active species, cobalt passes through the +1 oxidation state. We have since observed that with the same ligand the +3 oxidation state is still accessible as well (vide infra). This prompted us to investigate the possibility of using cobalt diimine pyridine complexes in hydrogenation catalysis (part of the work has appeared as a patent application [13]). Analogous Rh complexes [14] are included here for comparison.

* Corresponding author. Tel.: +31 24 3652186; fax: +31 24 3553450.
E-mail address: budz@sci.kun.nl (P.H.M. Budzelaar).

1381-1169/$ – see front matter © 2005 Elsevier B.V. All rights reserved.
doi:10.1016/j.molcata.2004.12.039

2. Experimental

2.1. General

All manipulations were carried out under an atmosphere of argon using standard Schlenk techniques or in a conventional nitrogen-filled glovebox. Solvents were refluxed over an appropriate drying agent and distilled prior to use. Hydrogenation specificity experiments were carried out in NMR tubes in C_6D_6 at room temperature under an inert atmosphere, using ca. 5 mg of Co complex. NMR spectra were recorded on Varian and Bruker spectrometers at ambient temperature. X-band EPR spectra were recorded on a Bruker ER 220. The spectra were simulated by iteration of the (an)isotropic *g* values, hyperfine coupling constants, and line widths.

The ligands L^{dip} [15] and L^{hex} [10] and the complexes $L^{dip}CoCl_2$ [15], $L^{hex}CoCl_2$ [10], $L^{dip}RhCl$ [16], $L^{dip}CoCH_2SiMe_3$ [12], $L^{hex}CoCH_2SiMe_3$ [10] and $L^{dip}RhMe$ [10] were synthesised following literature procedures. All other starting materials were obtained commercially and used as received.

2.2. $L^{dip}Co(CN)_3$

To 307 mg $L^{dip}CoCl_2$ (0.50 mmol) and 101 mg NaCN (2.06 mmol; 4.12 equiv.) 25 ml chloroform was added. No reaction had taken place even after 15 h of stirring. Addition of 2 ml H_2O resulted in a colour change from brown to red. Addition of a layer of hexane resulted in the precipitation of a dark red solid, which according to ^{1}H NMR consisted of a mixture of 65% $L^{dip}Co(CN)_3$ and 35% free L^{dip}. A similar experiment produced some crystals suitable for X-ray structure determination (see below). Attempts to obtain analytically pure samples by crystallization failed, so we do not have satisfactory elemental analysis data for this complex.

$L^{dip}Co(CN)_3$: ^{1}H NMR (200 MHz, $CDCl_3$): δ 8.61 (t, $^3J_{HH}$ 8 Hz, 1H, Py-*H4*), 8.34 (d, $^3J_{HH}$ 8 Hz, 2H, Py-*H3,5*), 3.36 (sept., $^3J_{HH}$ 6.5 Hz, 4H, ^{i}Pr-*H*), 2.46 (s, 6H, N=C-*Me*), 1.47 (d, $^3J_{HH}$ 6.5 Hz, 12H, ^{i}Pr-*Me*$_a$), 1.01 (d, $^3J_{HH}$ 6.5 Hz, 12H, ^{i}Pr-*Me*$_b$). IR (KBr): 2139 cm^{-1} (sh).

2.3. Reaction of metal-alkyl species with H_2

2.3.1. $L^{dip}CoCH_2SiMe_3$ and H_2

This reaction was reported earlier to produce $L^{dip}CoH$ [10]. The samples also show a weak EPR signal. Simulation yielded $g_\perp = 2.0285$, $g_\parallel = 1.996$, $A_{\perp(N)} = 10$ MHz, $A_{\parallel(Co)} = 30$ MHz (see Fig. S1). At room temperature, a g_{iso} value of 2.0112 was observed; we could not distinguish between a nitrogen superhyperfine coupling of 58.4 MHz or a cobalt hyperfine coupling of 22.4 MHz.

2.3.2. $L^{hex}CoCH_2SiMe_3$ and H_2

After addition of 2 ml of H_2, all ^{1}H NMR signals for $L^{hex}CoCH_2SiMe_3$ disappeared. At $T = 40$ K in toluene, an EPR signal was detected. Simulation yielded the following *g*-values and Co hyperfine couplings: $g_{11} = 1.9935$, $g_{22} = 1.9985$, $g_{33} = 2.0185$, $A_{11} = 77.7$ MHz, $A_{22} = 31.2$ MHz and $A_{33} = 26.8$ MHz.

2.3.3. $L^{dip}RhMe$ and H_2

After addition of 2 ml of H_2, all ^{1}H NMR signals for LRhMe disappeared. At $T = 40$ K in toluene, an EPR signal was detected. Simulation yielded $g_\parallel = 1.9775$, $g_\perp = 2.0169$, $A_{\parallel(Rh)} = 40$ MHz.

2.4. Hydrogenation of internal olefins

2.4.1. $L^{dip}CoCH_2SiMe_3$ and internal olefin

Eight milligrams of $L^{dip}CoCH_2SiMe_3$ and 8 mg 2-pentene were dissolved in 0.5 g C_6D_6 and a ^{1}H NMR spectrum was recorded. Two minutes after 1 ml of H_2 was injected, ^{1}H NMR showed a decrease in intensity of the vinylic protons around 5.4 ppm, indicating consumption of 2-pentene. Furthermore, the signals for $L^{dip}CoCH_2SiMe_3$ had disappeared, and, another Co^I complex had formed, which we identified as a Co^I *n*-pentyl species on basis of the ligand shifts (which resembled earlier reported Co^I alkyl species [12]) and the multiplet for the *n*-pentyl β-hydrogens at −0.8 ppm. After addition of an excess of H_2, ^{1}H NMR showed no traces of vinylic signals, indicating that all 2-pentene had been converted to pentane. Co was shown to be present in the form of $L^{dip}CoH$.

2.4.2. Selectivity of hydrogenation by $L^{dip}CoCH_2SiMe_3$ for α-olefin in the presence of trisubstituted olefin

Eight milligrams of $L^{dip}CoCH_2SiMe_3$ was dissolved in 0.5 g of C_6D_6, and 5 ml H_2 was added, resulting in the formation of $L^{dip}CoH$ as shown by ^{1}H NMR. Subsequently eight equivalents of 7-methyl-1,6-octadiene (MOD) were added. ^{1}H NMR showed that the signals for $L^{dip}CoCH_2SiMe_3$ had disappeared and a Co-alkyl complex had been formed through insertion of the terminal double bond of MOD into the Co–H bond (the ligand signals were again comparable to earlier observed alkyl species [12], and a multiplet for the alkyl β-hydrogens was observed at −0.8 ppm). After addition of more H_2, all terminal double bonds were hydrogenated, whereas the internal double bonds were still intact (only the signal at 5.3 ppm remained in the vinylic region, whereas the ones at 5.0 and 5.7 ppm associated with the terminal double bond had disappeared), and again $L^{dip}CoH$ was left.

2.4.3. $L^{hex}CoCH_2SiMe_3$ and internal olefin

$L^{hex}CoCH_2SiMe_3$ (6.9 mg) and 8 μl 2-hexene were dissolved in 2 ml hexane. To this solution 5 ml H_2 was added. ^{1}H NMR showed no traces of vinylic protons.

2.4.4. Selectivity of hydrogenation by $L^{hex}CoCH_2SiMe_3$ for α-olefin in the presence of trisubstituted olefin

Four milligrams of $L^{hex}CoCH_2SiMe_3$ and 10 μl 7-methyl-1,6-octadiene (MOD) were dissolved in 2 ml hexane. Ten millilitres of H_2 was added. ^{1}H NMR showed traces of the trisubstituted alkene bond, and other internal alkene

bonds (due to isomerisation products) but no monosubstituted alkene bond.

2.4.5. L^{dip}RhMe and internal olefin

Five milligrams of L^{dip}RhMe was dissolved in 0.6 ml C_6D_6 and placed in an NMR tube equipped with a septum. To the solution, 5 μl of a mixture of trans-2-hexene and cis-2-hexene was added after which a ^{1}H NMR spectrum was recorded. One millilitre of hydrogen was injected, the solution was stirred and a second ^{1}H NMR spectrum was recorded, which revealed that no vinylic protons were left, indicating that all hexene had been converted to hexane.

2.4.6. Selectivity of hydrogenation by L^{dip}RhMe for α-olefin in the presence of trisubstituted olefin

Selectivity of hydrogenation by L^{dip}RhMe for α-olefin in the presence of trisubstituted olefin was determined following a similar procedure, which revealed that the terminal alkene bond was hydrogenated (vinylic protons at 5.0 and 5.7 ppm had disappeared), whilst the trisubstituted one was not (5.3 ppm remained).

2.5. High pressure hydrogenation procedures

All products were identified and quantified by means of GC–MS.

2.5.1. Mechanically stirred reactor

The precatalyst was weighed into a Schlenk flask, which was then flushed with argon. TIBA (1 M in hexane) and 40 ml 1-octene were added and this reaction mixture was brought into a 100 ml pre-flushed steel autoclave. The mixture heated and maintained at 50 °C by means of a thermocouple. Twenty bar of hydrogen pressure was adjusted for 10 min. The reaction mixture was stirred mechanically by means of a gas-impelling stirrer.

2.5.2. Magnetically stirred reactor

A 100 ml glass autoclave (miniclave, Büchi AG) was baked out at 150 °C and cooled to ambient temperature in a nitrogen atmosphere. TIBA (0.5 ml 1 M in hexane), the catalyst and 1-octene (10 ml, solvent as well as substrate) were introduced in that order. The reactor was heated to 50 °C in an oil bath, after which a constant 5 bar hydrogen pressure was adjusted for 10 min. The reaction mixture was stirred with a magnetic stirring bar at 200 rpm. To measure the decay of activity, experiments were carried out under a 2-bar hydrogen pressure in the same autoclave setup, enabling sampling through a septum without stopping the experiment.

2.6. Calculations

Density functional calculations were performed with the TURBOMOLE program [17–19] in combination with the OPTIMIZE routine of Baker and co-workers [20,21]. All relevant minima and transition states were fully optimised at the unrestricted b3-lyp level [22–25] employing the standard SV(P) basis sets [26] and a small-core pseudopotential for Co [27]. Numerical or analytical second derivatives were calculated for all stationary points, and thermal corrections (enthalpy and entropy, 323 K, 20 bar) were calculated from these to produce the final relative free energies mentioned in the text.

Table 1
Crystallographic data for $L^{dip}Co(CN)_3$

Compound	$L^{dip}Co(CN)_3$
Crystal colour	Transparent dark red
Crystal shape	Rough platelet
Crystal size (mm^3)	$0.38 \times 0.11 \times 0.03$
Empirical formula	$C_{36}H_{43}CoN_6 \cdot 4H_2O$
Formula weight	690.76
Temperature (K)	293(2)
Radiation/wavelength (Å)	MoKα (graphite mon.)/0.71073
Crystal system, space group	Triclinic, P-1
Unit cell dimensions	$a = 15.409(3)$ Å, $\alpha = 108.592(15)^\circ$ $b = 15.472(4)$ Å, $\beta = 101.604(15)^\circ$ $c = 17.244(3)$ Å, $\gamma = 105.549(15)^\circ$
Volume (Å^3)	3563.9(13)
105275 reflections	
Z, calculated density (mg/m^3)	4, 1.287
Absorption coefficient (mm^{-1})	0.528
Diffractometer/scan	Nonius KappaCCD with area detector θ and ω scan
$F(0\,0\,0)$	1472
θ range for data collection (°)	4.99–25.00
Index ranges	$-18 \le h \le 18$, $-18 \le k \le 18$, $-20 \le l \le 20$
Reflections collected/unique	105275/12462 [R(int) = 0.0951]
Reflections observed	8113 [$I_o > 2\sigma(I_o)$]
Absorption correction	SADABS multiscan correction [31]
Refinement method	Full-matrix least-squares on F^2
Computing	SHELXL-97 [32]
Data/restraints/parameters	12462/0/835
Goodness-of-fit on F^2	1.064
SHELXL-97 weight parameters	0.0710, 3.4334
Final R indices [$I > 2\sigma(I)$]	R1 = 0.0571, wR2 = 0.1362
R indices (all data)	R1 = 0.1063, wR2 = 0.1600
Largest diff. peak and hole	1.079 and −0.286 e Å^{-3}

2.7. X-ray structure determination for $L^{dip}Co(CN)_3$

The crystal data and a summary of the data collection and structure refinement are given in Table 1 (for further details, see Tables S2–S5 of the supplementary data). The structure was solved by the PATTY option [28] of the DIRDIF program system [29]. All nonhydrogen atoms were refined with anisotropic temperature factors. The hydrogen atoms were placed at calculated positions, and refined isotropically in riding mode. The structure is shown in Fig. 1 [30]. The structure consists of two independent molecules. In addition, four significant, isolated electron densities were found in the difference Fourier map. These were treated as disordered, partially occupied water molecules. No hydrogen atoms could be located for these oxygen atoms, so no hydrogen bonds could be detected which would support this assignment. This

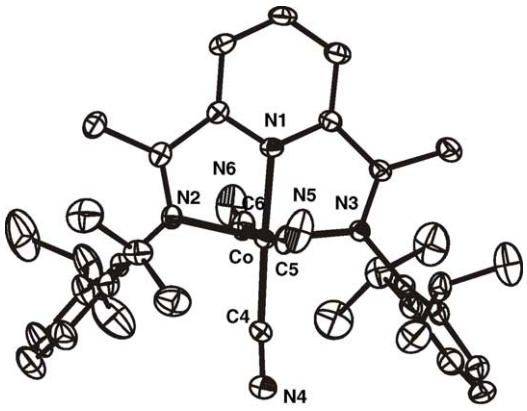

Fig. 1. ORTEP image of the X-ray structure of $L^{dip}Co(CN)_3$, drawn at 30% probability; hydrogen atoms are omitted for clarity.

means that the chemical nature of these atoms is questionable. Finally, a void of 60 Å^3 was found in the structure in the neighbourhood of O103. The SQUEEZE procedure showed no net electron density in this void [30] although there are some low residual electron densities in the difference Fourier map. Geometrical calculations [30] revealed neither unusual geometric features, nor unusual short intermolecular contacts. The calculations revealed no higher symmetry and no further solvent accessible areas.

3. Results and discussion

3.1. Synthesis and characterisation of Co(I) complexes

The ligands L^{dip} and L^{hex} (Fig. 2) are prepared from the condensation of two equivalents of the appropriate aniline or amine with diacetylpyridine. For cobalt, the dichloride complexes are synthesised in THF under air. The reduction and subsequent alkylation from $L^{hex}CoCl_2$ to $L^{hex}CoCH_2SiMe_3$ is achieved in one step using two equivalents of $LiCH_2Me_3$ [10]. $L^{dip}CoCH_2SiMe_3$ [12] and $L^{dip}RhMe$ [14] were synthesised according to literature procedures.

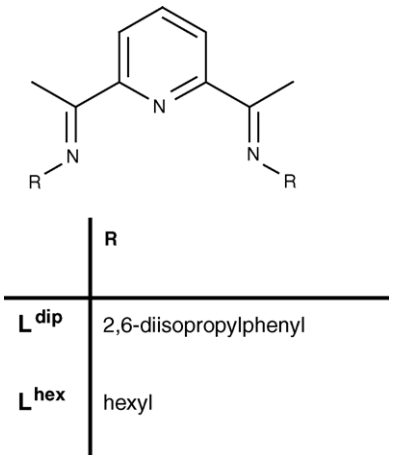

Fig. 2. Diiminepyridine ligands used.

3.2. Synthesis of $L^{dip}Co(CN)_3$

This product was not used in hydrogenation experiments, but is included here to demonstrate that the +3 oxidation state is accessible for Co in its complexes with L^{dip}. The reaction of $L^{dip}CoCl_2$ with NaCN in water/chloroform under air produced $L^{dip}Co(CN)_3$. Layering with hexane produced crystals that were suitable for X-ray diffraction. Fig. 1 shows one of the two independent molecules present in the unit cell. The Co^{III} center atom has a distorted octahedral geometry with an N1–Co–N3 angle of 162.66(12)°. This distortion is imposed by the ligand geometry and is also observed for other octahedral cobalt complexes bearing this type of ligand [7]. Furthermore, the two apical cyanides are bent away from the equatorial one, presumably due to steric repulsion with the bulky diisopropylphenyl groups, resulting in angles C5–Co–C6 = 172.7(2)°, Co–C5–N5 = 170.6(4)°, Co–C6–N6 = 167.0(4)° (compare with Co–C4–N4 = 175.2(4)°). The Co–C distances (Co–C4 = 1.894(4), Co–C5 = 1.906(5), Co–C6 = 1.898(5)) are similar to those found in other low-spin Co(III) cyanides [33–36]. The IR spectrum shows a single, sharp IR band at 2139 cm^{-1}, which presumably represents coincident $\nu_{as}(CN)_{ax}$ and $\nu(CN)_{eq}$ transitions (the $\nu_s(CN)_{ax}$ transition is expected to have a very low intensity). In related amine complexes of $Co(CN)_3$, ν(CN) tends to be slightly smaller (2127 cm^{-1} for a fac complex [35]; 2129/2133/2145 cm^{-1} for a mer complex [34]).

3.3. Hydrogenation with $L^{dip}Co$ complexes [37]

Reaction of $L^{dip}CoCH_2SiMe_3$ with H_2 produces a diamagnetic complex, which we believe to be the hydride $L^{dip}CoH$ on the basis of ^{1}H NMR [10].

Monosubstituted olefins easily insert into the Co–H bond of this hydride to form the corresponding alkyl derivatives. Upon addition of more H_2, the alkyl group is hydrogenated off as an alkane and the hydride species is regenerated (Scheme 1) [13]. Similarly, Gibson et al. [38] showed that in the reaction of $L^{dip}CoMe$ with hydrogen a species is formed believed to be $L^{dip}CoH$, and which reacted with ethylene to give $L^{dip}CoEt$. 1,2-Disubstituted olefins can also insert and be hydrogenated. For example, reaction of 2-pentene with

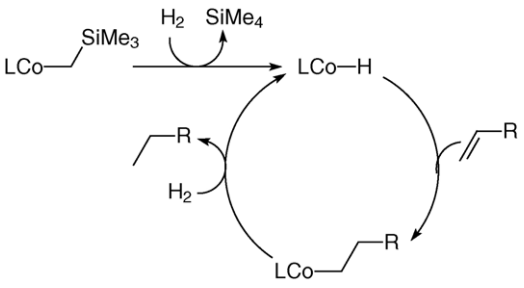

Scheme 1. Hydrogenation cycle as followed by ^{1}H NMR for $L^{dip}CoR$.

$L^{dip}CoH$ produces the *n*-pentyl complex, which then forms pentane in the presence of excess hydrogen. This demonstrates that alkyls can be isomerised at the cobalt center prior to hydrogenation. Trisubstituted olefins, however, do not react, showing that the hydrogenation activity is sensitive to steric factors. This is illustrated by the hydrogenation of 7-methyl-1,6-octadiene (MOD): only the monosubstituted C=C bond was hydrogenated. For catalytic hydrogenation, it is more convenient to use $L^{dip}CoCl_2$ and activate it in situ with TIBA (triisobutylaluminum), as discussed in more detail below.

3.4. Hydrogenation with $L^{hex}Co$ complexes

In polymerisation with diiminepyridine complexes of Co and Fe, steric shielding of the metal by bulky aryl substituents is necessary to obtain high molecular weight polymers [15,39-41]. In order to test whether this type of shielding is also needed for hydrogenation, complex $L^{hex}CoCH_2SiMe_3$ [10], which carries *n*-hexyl groups on the imines, was tested in hydrogenation. The product of the reaction between $L^{hex}CoCH_2SiMe_3$ and H_2 is not the expected hydride $L^{hex}CoH$ but a paramagnetic species that shows a clear EPR signal (see below) and is NMR-silent. Despite this difference in behaviour between L^{dip} and L^{hex} complexes, catalytic hydrogenation using $L^{hex}CoCl_2$/TIBA shows an activity and specificity similar to that of $L^{dip}CoCl_2$/TIBA.

3.5. Hydrogenation with $L^{dip}Rh$ complexes

$L^{dip}RhMe$ also reacts with H_2 to form a paramagnetic and NMR-silent product [14]. Catalytic hydrogenation using $L^{dip}RhCl$/TIBA shows a specificity with MOD similar to that of the Co complexes.

3.6. EPR measurements.

The paramagnetic product of $L^{hex}CoCH_2SiMe_3$ and H_2 shows a clear EPR signal indicative of an S = 1/2 species. The rhombic signal (Fig. 3) could be simulated satisfactorily using only hyperfine coupling to Co.

On closer inspection we found that also in the reaction between $L^{dip}CoCH_2SiMe_3$ and H_2, besides $L^{dip}CoH$, some paramagnetic product is formed (at most 5% according to a quantitative ^1H NMR experiment). In this case, interpretation of the EPR signal is less straightforward. The spectrum in toluene glass ($T = 40$ K) shows a broad signal indicative of axial symmetry ($g_{\|} = 2.0825$, $g_{\perp} = 1.997$) (spectrum: Fig. S1, in supplementary data). At room temperature, the isotropic signal at $g = 2.0112$ (Fig. 4) reveals some (super)hyperfine coupling; we cannot unambiguously discriminate between a superhyperfine coupling to a single nitrogen ($A_{iso(N)} \approx 58$ MHz, Fig. 4A) and a cobalt hyperfine coupling ($A_{iso(Co)} \approx 22$ MHz, Fig. 4B), although the former gives a slightly better fit. The observation of isotropic signals

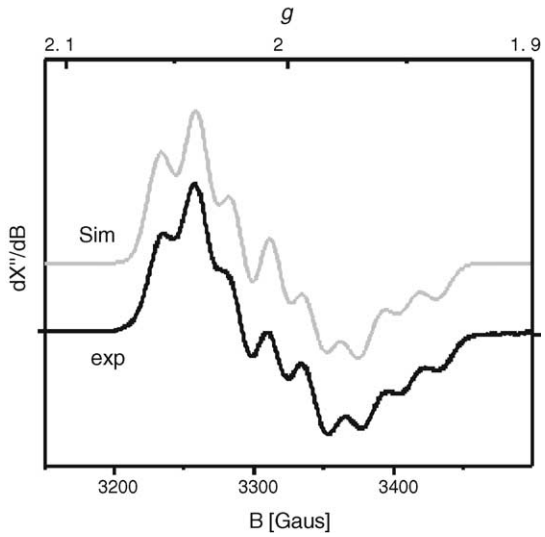

Fig. 3. EPR of reaction product of $L^{hex}CoCH_2SiMe_3$ and H_2 (toluene glass, 40 K). Simulation: $g_{11} = 1.9935$, $g_{22} = 1.9985$, $g_{33} = 2.0185$, $A_{11(Co)} = 77.7$ MHz, $A_{22(Co)} = 31.2$ MHz and $A_{33(Co)} = 26.8$ MHz.

at r.t. as seen for $L^{dip}CoR + H_2$ is indicative of mainly ligand-centred radicals

It is remarkable that upon reaction with H_2 $L^{hex}CoR$ generates exclusively a paramagnetic complex, while for $L^{dip}CoR$ the paramagnetic product is only a minor product. For both ligands, the paramagnetic complex is probably a low-spin $L^{\bullet -}Co$ ligand radical complex (in which $L^{\bullet -}$ denotes the radical anion of L), where the unpaired electron is delocalised to the metal to different extents. Acces to the paramagnetic species seems to be promoted by the decreased steric bulk of the L^{hex} ligand compared to L^{dip}. The exact nature of these paramagnetic species cannot be derived from the EPR spectra.

The EPR spectrum of the paramagnetic product obtained from $L^{dip}RhMe$ and H_2 (toluene glass, 40 K) shows an axial signal indicative of an S = 1/2 species, of which $g_{\|}$ reveals superhyperfine coupling; simulation yields $g_{\|} = 1.9775$, $g_{\perp} = 2.0169$, $A_{\|(N)} = 40$ MHz [14]. Since the *g*-values of the paramagnetic rhodium species are close to g_e, it seems logical to assume that the unpaired electron is mainly located on a ligand fragment, presumably in one of the pyridine 2,6-diimine π^* orbitals. This would imply a formulation as $L^{\bullet -}Rh^{I}$ or $L^{\bullet -}Rh^{III}H_2$.

3.7. Hydrogenation activity

Rates of hydrogenation were determined with 1-octene as substrate and solvent. In general, the dichloride (cobalt) or monochloride (rhodium) precursors were used (0.2–25 μmol) in combination with a large excess of TIBA (typically 0.5 mmol) as activator and scavenger. TIBA (1 M in hexane) was first added to the solid precursor, since the activated catalyst dissolves in hexane (and 1-octene). For low

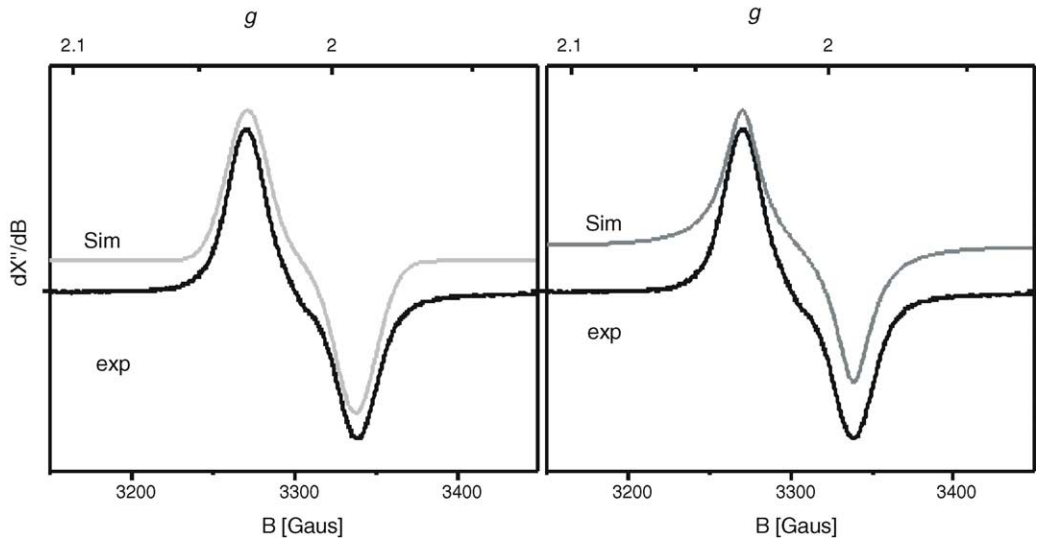

Fig. 4. EPR of reaction product of $L^{dip}CoCH_2SiMe_3$ and H_2 (room temperature). Simulation: g_{iso} = 2.0112; (A) $A_{iso(N)}$ = 58.4 MHz; (B) $A_{iso(Co)}$ = 22.4 MHz.

intake experiments this solution was further diluted and extra TIBA was added in order to maintain the same scavenger concentration. Control experiments using pre-formed metal alkyls showed that in situ activation by TIBA was effective. Hydrogenation rates at low intake (ca. 0.5 μmol catalyst, glass autoclave, magnetic stirring, 5 bar H_2) showed conversion of 1-octene by $L^{dip}CoCl_2$, $L^{hex}CoCl_2$ and $L^{dip}RhCl$ with TIBA in the order of 10,000 mol/mol catalyst/bar/h. For $L^{dip}CoCl_2$, conversion was found to vary linearly with hydrogen pressure in the range of 5–50 bar (see Table S1 and Figs. S2–S4 in supplementary data for details of all experiments).

However, conversion did not depend linearly on catalyst intake. The possibility that this might be due to diffusion limitation was ruled out by experiments using $L^{dip}CoCl_2$ in a mechanically stirred reactor at 20 bar. In this setup, hydrogen was added efficiently directly into the octene by means of a gas-impelling stirrer. Stirring at full or half capacity gave the same conversion.

Fig. 5 shows the results for four separate experiments using varying amounts of catalyst (further results under a variety of stirring conditions and pressures are listed in Table S1 of the supplementary data). The graph clearly shows that higher catalyst intake leads to lower turnovers. Such behaviour is sometimes observed if the catalyst is sensitive to the product. In the present case, where the product is a saturated alkane, this is highly unlikely. Therefore, we suspect that a bimolecular catalyst deactivation may be responsible [42].

For $L^{dip}CoCl_2$, the decay of activity with time was measured as well. The magnetically stirred setup was loaded with a large amount of catalyst, and a hydrogen pressure of two bar was maintained for one hour. This low pressure enabled sampling through a septum. Conversion was monitored by taking GC samples at 10-min intervals (Fig. 6). Some form of catalyst decay is obvious from these data. The solid and dashed lines in the figure are least-squares fits assuming second-

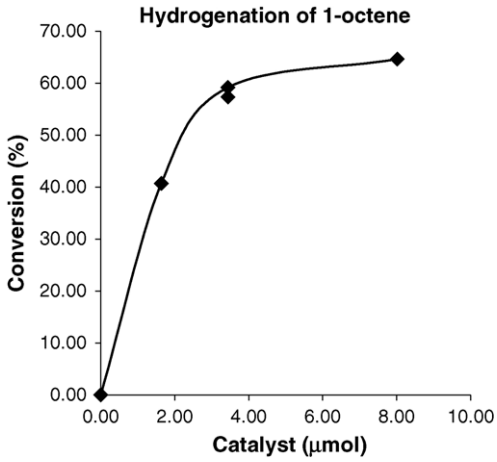

Fig. 5. Conversion versus intake ($L^{dip}CoCl_2$, mechanical stirring, 20 bar H_2).

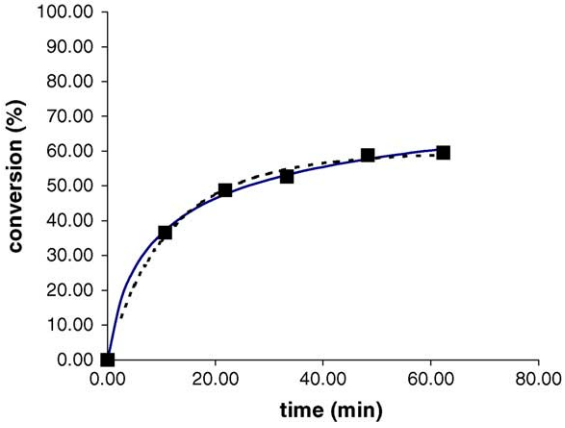

Fig. 6. Conversion vs. time for hydrogenation of 1-octene with $L^{dip}CoCl_2$, fitted assuming second-order (solid line) or first-order (dashed line) catalyst decay.

order and first-order catalyst decay, respectively. The fit is marginally better for the second-order model, but the data are not good enough to allow discrimination between the two models.

3.8. Theoretical studies

In order to shed more light on the possible mechanism(s) of the hydrogenation catalysis, we have studied the reaction using DFT methods. Both Co^{I} and $Co^{(0)}$ cycles were considered. Fig. 7 shows the free energy profiles calculated for the two cycles using a simple ligand model (H substituents only) and ethylene as the model substrate.

The relative free energies for the species occurring in the hydrogenation cycles of Fig. 7 are listed in Table 2 (total energies and low frequencies are listed in Table S6).

The Co^{I} cycle is straightforward. Ethylene coordinates weakly to LCoH (**1**) and then inserts with a low barrier to give Co^{I} alkyl **4**. This then coordinates H_2, but does not cleave the H–H bond [43]. Ethane formation proceeds through direct transfer of one of the H_2 hydrogens of **5** to the ethyl group, i.e. this step should be considered as a σ-bond metathesis reaction rather than an oxidative addition/reductive elimination sequence. Thus, even though we have demonstrated that for Co coordinated to L^{dip} the +3 oxidation state is accessible, it is apparently not needed in this hydrogenation cycle. The rate-determining step of the cycle is the σ-bond metathesis step, with an activation energy (relative to LCoEt) of about 21 kcal/mol [44].

The $Co^{(0)}$ cycle starts with LCo. Of the two possible initial reactions, complexation of ethylene or H_2, the former is strongly preferred. After ethylene coordination, binding of H_2 to form $LCo(C_2H_4)(H)_2$ is strongly endothermic. Once this complex has been formed, both ethylene insertion and subsequent reductive ethane elimination have low barriers. The rate-determining step of this cycle is ethylene insertion, with a barrier (relative to $LCo(C_2H_4)$ **13**) of ca. 30 kcal/mol, i.e. somewhat higher than found for the Co^{I} cycle.

Both cycles require approximately the same amount of space around the metal, so steric effects should be similar. Based on the computational results, it seems that the Co^{I} cycle is likely to be the most important one, which at least for L^{dip} is in agreement with the experimental results [45].

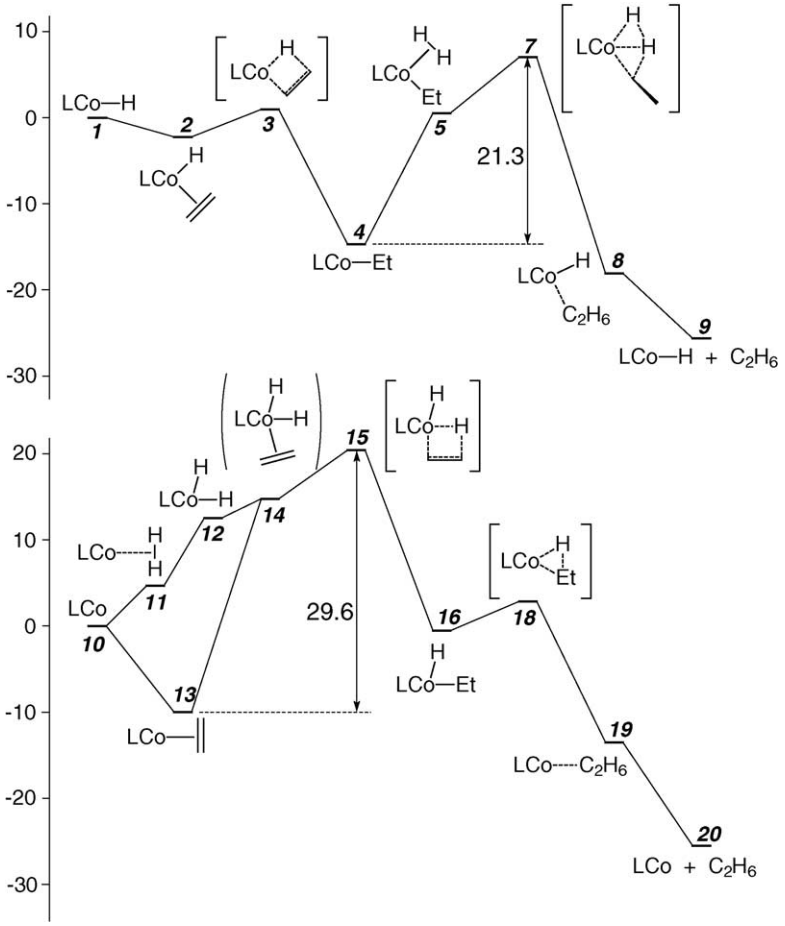

Fig. 7. Free energy profiles (kcal/mol) for Co^{I}/Co^{III} and $Co^{(0)}/Co^{II}$ hydrogenation cycles.

Table 2
Relative free energies for species in the two hydrogenation cycles

	Complex	E_{rel} (kcal/mol)
Co^{I} cycle		
1	LCoH	(0)[a]
2	$LCoH(C_2H_4)$	−2.76
3	$LCo(H\cdots C_2H_4)$	0.30
4	LCoEt	−15.41[a]
5	$LCo(Et)(H_2)$	−0.58[b]
6	$LCo(Et)(H)_2$	–[c]
7	$LCo(Et\cdots H\cdots H)$	5.87
8	$LCoH(C_2H_6)$	−19.12
9	$LCoH + C_2H_6$	−26.28
$Co^{(0)}$ cycle		
10	LCo	(0)
11	$LCo(H_2)$	4.10
12	$LCo(H)_2$	–[d]
13	$LCo(C_2H_4)$	−10.84
14	$LCo(C_2H_4)(H)_2$	–[e]
15	$LCo(H\cdots H\cdots C_2H_4)$	18.76
16	LCo(H)(Et) (H apical)	−2.20
17	LCo(H)(Et) (Et apical)	0.60
18	$LCo(H\cdots Et)$	1.33
19	$LCo(C_2H_6)$	−14.81
20	$LCo + C_2H_6$	−26.28

[a] Singlet biradical, prefers a broken-symmetry solution. For details see Ref. [10].
[b] Regular local minimum on the restricted b3-lyp surface. However, only about 0.2 kcal/mol above this minimum in the direction of H_2 dissociation, the broken-symmetry solution becomes more stable, and then the energy decreases monotonically to **4**.
[c] Not a local minimum, collapses to H_2 complex **5**.
[d] Very shallow minimum, ca. 7.7 kcal/mol above **11**, with a barrier <0.1 kcal/mol for collapse back to **11**.
[e] Not a local minimum, but on a very flat plateau ca. 1.3 kcal/mol below **15**.

4. Conclusions

The square planar Co^{I} alkyl species that were recently discovered as intermediates in the activation pathway for the polymerisation of ethylene are also active catalysts for the hydrogenation of olefins. Introduction of less bulky substituents at the imine nitrogens does not affect this catalyst activity much, in contrast to the ligand effects observed in polymerisation [15,39–41]. Establishing the active species is difficult for any catalytic reaction. In the case of the $L^{dip}Co$ catalyst, stoichiometric experiments have demonstrated both olefin insertion into the hydride and hydrogenolysis of the metal-alkyl bond, supporting a cycle involving $L^{dip}CoH$. However, the fact that also a small amount of paramagnetic product (<5%) is formed upon reaction with H_2 means that the possibility of a paramagnetic species being active as well cannot be ruled out. Calculations are not conclusive but indicate a cycle involving $L^{dip}CoH$ is reasonable. This shows that, given the right ligand environment, Co can indeed be made to display “rhodium-like” catalysis.

Acknowledgements

We thank Prof. D. Vogt and Dr. C. Müller for helpful discussion on the subject of diffusion limitation, and for the use of the mechanically stirred autoclave setup for high-pressure hydrogenation experiments. We are grateful to Dr. M.G. Nijkamp and Drs. M.M.P. Grutters for their assistance with the use this equipment. We thank Dr. F. Neese for a copy of his EPR simulation program.

Appendix A. Supplementary data

Supplementary data associated with this article can be found, in the online version, at 10.1016/j.molcata.2004.12.039.

EPR spectrum measured at 40 K of the reaction between $L^{dip}CoCH_2SiMe_3$ and H_2 (Fig. S1), full experimental details about additional hydrogenation runs (Table S1, Figs. S2–S4), crystallographic data for $L^{dip}Co(CN)_3$ (Tables S2–S5), total energies, thermal corrections and lowest frequencies for species studied theoretically (Table S6)

Crystallographic data (excluding structure factors) for $L^{dip}Co(CN)_3$ have been deposited with the Cambridge Crystallographic Data Centre as supplementary publication CCDC 237217. Copies of available material can be obtained, free of charge, on application to the Director, CCDC, 12 Union Road, Cambridge CB2 1EZ, UK, (fax: +44 1223 336033 or e-mail: teched@chemcrys.cam.ac.uk).

References

[1] B. Cornils, W.A. Herrmann, Applied Homogenous Catalysis with Organometallic Compounds, Weinheim, 1996.
[2] G.W. Parshall, S.D. Ittel, Homogenous Catalysis, second ed., John Wiley, New York, 1992.
[3] Ref. [1], section 2.1.1.
[4] Ref. [2], section 5.4.
[5] Ref. [1], section 2.2.
[6] Ref. [2], chapter 3.
[7] B. De Bruin, E. Bill, E. Bothe, T. Weyhermuller, K. Wieghardt, Inorg. Chem. 39 (2000) 2936.
[8] P.H.M. Budzelaar, B. De Bruin, A.W. Gal, K. Wieghardt, J.H. Van Lenthe, Inorg. Chem. 40 (2001) 4649.
[9] H. Sugiyama, G. Aharonian, S. Gambarotta, G.P.A. Yap, P.H.M. Budzelaar, J. Am. Chem. Soc. 124 (2002) 12268.
[10] Q. Knijnenburg, D. Hetterscheid, T.M. Kooistra, P.H.M. Budzelaar, Eur. J. Inorg. Chem. 6 (2004) 1204.
[11] V.C. Gibson, M.J. Humphries, K.P. Tellmann, D.F. Wass, A.J.P. White, D.J. Williams, Chem. Commun. 21 (2001) 2252.
[12] T.M. Kooistra, Q. Knijnenburg, J.M.M. Smits, A.D. Horton, P.H.M. Budzelaar, A.W. Gal, Angew. Chem. Int. Ed. Engl. 40 (2001) 4719.
[13] A.D. Horton, Q. Knijnenburg, H. van der Heijden, P.H.M. Budzelaar, A.W. Gal, WO 03042131 (2003); EP 2001-204376 (2001).
[14] T.M. Kooistra, D.G.H. Hetterscheid, E. Schwartz, Q. Knijnenburg, P.H.M. Budzelaar, A.W. Gal, Inorg. Chim. Acta 357 (2004) 2945.
[15] G.J.P. Britovsek, M. Bruce, V.C. Gibson, B.S. Kimberley, P.J. Maddox, S. Mastroianni, S.J. McTavish, C. Redshaw, G.A. Solan, S.

Strömberg, A.J.P. White, D.J. Williams, J. Am. Chem. Soc. 121 (1999) 8728.
[16] H.F. Haarman, J.M. Ernsting, M. Krananburg, H. Kooijman, N. Veldman, A.L. Spek, P.W.N.M. van Leeuwen, K. Vrieze, Organometallics 16 (1997) 887.
[17] R. Ahlrichs, M. Bär, M. Häser, H. Horn, C. Kölmel, Chem. Phys. Lett. 162 (1989) 165.
[18] O. Treutler, R. Ahlrichs, J. Chem. Phys. 102 (1995) 346.
[19] R. Ahlrichs, M. Bär, H.-P. Baron, R. Bauernschmitt, S. Böcker, M. Ehrig, K. Eichkorn, S. Elliott, F. Furche, F. Haase, M. Häser, C. Hättig, H. Horn, C. Huber, U. Huniar, M. Kattannek, A. Köhn, C. Kölmel, M. Kollwitz, K. May, C. Ochsenfeld, H. Öhm, A. Schäfer, U. Schneider, O. Treutler, K. Tsereteli, B. Unterreiner, M. von Arnim, F. Weigend, P. Weis, H. Weiss Turbomole Version 5, January 2002. Theoretical Chemistry Group, University of Karlsruhe.
[20] PQS version 2.4, 2001. Parallel Quantum Solutions, Fayetteville, Arkansas, USA (the Baker optimizer is available separately from PQS upon request).
[21] J. Baker, J. Comput. Chem. 7 (1986) 385.
[22] C. Lee, W. Yang, R.G. Parr, Phys. Rev. B 37 (1988) 785.
[23] A.D. Becke, J. Chem. Phys. 98 (1993) 1372.
[24] A.D. Becke, J. Chem. Phys. 98 (1993) 5648.
[25] All calculations were performed using the Turbomole functional "b3-lyp", which is not identical to the Gaussian "B3LYP" functional.
[26] A. Schäfer, H. Horn, R. Ahlrichs, J. Chem. Phys. 97 (1992) 2571.
[27] D. Andrae, U. Haeussermann, M. Dolg, H. Stoll, H. Preuss, Theor. Chim. Acta 77 (1990) 123.
[28] P.T. Beurskens, G. Beurskens, M. Strumpel, C.E. Nordman, in: J.P. Glusker, B.K. Patterson, M. Rossi (Eds.), Patterson and Pattersons, Clarendon Press, Oxford, 1987, p. 356.
[29] P.T. Beurskens, G. Beurskens, W.P. Bosman, R. de Gelder, S. Garcia-Granda, R.O. Gould, R. Israel, J.M.M. Smits, DIRDIF-96. A computer program system for crystal structure determination by Patterson methods and direct methods applied to difference structure factors, Crystallography Laboratory, University of Nijmegen, The Netherlands, 1996.
[30] A.L. Spek, PLATON. A Multipurpose Crystallographic Tool, Utrecht University, Utrecht, The Netherlands, 2003.
[31] G.M. Sheldrick, SADABS. Program for Empirical Absorption Correction, University of Gottingen, Germany, 1996.
[32] G.M. Sheldrick, SHELXL-97. Program for the refinement of crystal structures, University of Gottingen, Germany, 1997.
[33] M. Ishii, M. Umehara, M. Nakahara, Bull. Chem. Soc. Jpn. 60 (1987) 125.
[34] H. Chun, E.M. Maes, R.S. Czernuszewicz, I. Bernal, Polyhedron 20 (2001) 2597.
[35] J.Y. Yang, M.P. Shores, J.J. Sokol, J.R. Long, Inorg. Chem. 42 (2003) 1403.
[36] H. Chun, I. Bernal, Cryst. Growth Des. 1 (2001) 143.
[37] After the present work was submitted, an experimental/theoretical study of the Co^{I} path of olefin hydrogenation with $L^{dip}Co$ appeared K.P. Tellmann, M.J. Humphries, H.S. Rzepa, V.C. Gibson, Organometallics 23 (2004) 5503.
[38] V.C. Gibson, K.P. Tellmann, M.J. Humphries, D.F. Wass, Chem. Commun. 20 (2002) 2316.
[39] B.L. Small, M. Brookhart, A.A. Bennett, J. Am. Chem. Soc. 120 (1998) 4049.
[40] G.J.P. Britovsek, V.C. Gibson, B.S. Kimberley, P.J. Maddox, S.J. McTavish, G.A. Solan, A.J.P. White, D.J. Williams, Chem. Commun. 18 (1998) 849.
[41] B.L. Small, M. Brookhart, J. Am. Chem. Soc. 120 (1998) 7143.
[42] Catalyst preparation times were kept constant. If catalyst decomposition was first-order, initial rates should not be affected by it.
[43] The ethyl-dihydride complex LCo(Et)(H)2 was found not te be a local minimum; it rearranges spontaneously to the dihydrogen complex LCo(Et)(H2).
[44] This should be considered as a rough estimate only. LCoEt prefers a broken-symmetry ub3-lyp solution. In the present work we have used the ub3-lyp energies throughout, but for an accurate energy estimate one would need a "true singlet" energy of this and similar species. See, e.g. Ref. [8].
[45] One could assert that the formation of paramagnetic species from LhexCoR and LdipRhR and H2 argues against an M^{I} cycle for these two precursors. However, if paramagnetic ($M^{(0)}$ or M^{II}) species are easily formed from M^{I} precursors, the reverse reaction is also possible, so diamagnetic cycles are still possible even for these two systems.